The load-bearing elements of a number of strategic equipment are of limited length and variable cross-section. Most of them are exposed to certain types of heat sources. In order to ensure the reliable operation of this equipment, it is necessary to know the temperature field along the length of the variable cross-section rod. In this paper, a computational algorithm and a method for determining the temperature field along the length of a rod with a limited length and variable cross-section are proposed. They are based on the fundamental laws of conservation of energy.

The nonlinearity of the process is due to nonlinear dependencies of the areas of the variable cross-section on the coordinate. The radius of the cross-section of the rod decreases linearly along the entire length, starting from the left end. The side surface of the first and third discrete elements of the rod is heat-insulated. Convective heat exchange with the environment takes place on the side surface of the second discrete element of the rod.

The cross-sectional area of the left end of the rod is under the heat flow with a constant intensity, and a heat flow with different intensities is supplied to the right end, wherein the heat transfer coefficient is considered constant. For this task, you must first determine the law of temperature distribution along the length of the rod. In addition, if one end is rigidly fixed and the other end is free, the elongation must be calculated depending on the available heat sources, the physical and geometric characteristics of the rod, taking into account the presence of insulation.

In case of pinching of both ends of the investigated rod, the value of axial compressive force is calculated taking into account the addition of real factors. The distribution of all components of the strain, stress, and displacement field is also defined

Keywords: heat flux intensity, thermal conductivity coefficient, temperature, heat transfer coefficient

UDC 004.94

DOI: 10.15587/1729-4061.2023.273635

DEVELOPING A METHOD OF ACCOUNTING FOR THE EXISTENCE OF LOCAL SURFACE HEAT EXCHANGE IN RODS OF VARIABLE CROSS-SECTION

Mukaddas Arshidinova
Corresponding author
Doctoral Candidate
Department of IT
Al-Farabi Kazakh National University
Al-Farabi ave., 71, Almaty, Republic of Kazakhstan, 05059
E-mail: mukaddas_arshidi@mail.ru
Azat Tashev
Doctor in Technical Sciences*
Anarbay Kudaykulov
Doctor in Physics and Mathematics*
*Department of IT
Institute of Information and Computational Technologies
Shevchenko str., 28, Almaty, Republic of Kazakhstan, 050010

Received date 10.01.2023
Accepted date 29.03.2023
Published date 30.06.2023

How to Cite: *Arshidinova, M., Tashev, A., Kudaykulov, A. (2023). Developing a method of accounting for the existence of local surface heat exchange in rods of variable cross-section. Eastern-European Journal of Enterprise Technologies, 3 (7 (123)), 53–64. doi: https://doi.org/10.15587/1729-4061.2023.273635*

1. Introduction

Consider a horizontal core of limited length L (cm) and variable cross-section $F(x)$ (cm^2). The radius of the core section changes linearly along its length $r=ax+b$ (cm), $(0\le x\le L)$, where a and b are constants. The cross-sectional area of the core changes not linearly along the core length as follows $F(x)=\pi r^2=\pi(a^2x^2+2abx+b^2)$ (cm^2), $(0\le x\le L)$.

The physical and mechanical properties of the core material are characterized by the heat conductivity coefficient $K_{xx}\left(\frac{\text{watt}}{\text{cm}\cdot{}^\circ\text{K}}\right)$, and thermal expansion $\alpha\left(\frac{1}{{}^\circ\text{K}}\right)$ module of elasticity of the core material $E\left(\frac{\text{kg}}{\text{cm}^2}\right)$. Let us assume that on the cross-sectional area of the left end of the core, the heat flux of constant intensity is brought $q_1\left(\frac{\text{watt}}{\text{cm}^2}\right)$. At this time, on the cross-sectional area of the right end of the core, the heat flux is brought with intensity $q_2\left(\frac{\text{watt}}{\text{cm}^2}\right)$. Local side surfaces $(0\le x\le L_1)$ and $(L_2\le x\le L)$ of the studied core are heat-insulated. Through the local side surface $(L_1\le x\le L_2)$ of the core, there is a heat exchange to the environment. At the same time, with the heat exchange coefficient $h\left(\frac{\text{watt}}{\text{cm}^{2\circ}\text{K}}\right)$, and ambient temperature T_{oc} (°K), it is necessary to define the field of distribution of temperature, three components of strain, stress and displacement.

The existing methods of studying the thermomechanical state of a rod of variable cross-section take into account the influence of individual external factors on the distribution of body temperature: either heat insulation, or heat exchange with the environment or heat flow and temperature. Therefore, the problem of developing a mathematical model of the thermomechanical state of a rod of variable cross-section, which would take into account the simultaneous influence of local temperature, thermal insulation and heat exchange with the external environment, is relevant.

2. Literature review and problem statement

The definition of the law of temperature distribution along the length of the rod elements is relevant, since in the

bearing components of power plants, internal combustion engines and hydrogen engines during operation, a thermal stress state is manifested. The work outlines the basics of the theory of elasticity, with solutions to practical engineering problems [1]. The paper [2] presents calculation methods and algorithms for the numerical solution of a class of applied mechanics problems.

The main equations of thermo-physics, including the laws of conservation of mass, momentum and energy, are given in [3]. This paper provides kinematic equations as well as corresponding relations that close the systems of equations. The analysis of the work shows that, first, the existing methods of studying the thermomechanical state of the bearing elements of structures take into account the influence of individual external factors on the distribution of body temperature: either heat insulation, or heat exchange with the environment or heat flow and temperature.

Fundamental theoretical issues concerning thermo-physics are given in [4, 5]. In [6], the contact heat transfer characteristics at the interface of a distributed rotor rod mount interface, under different influences and taking into account the roughness of different wheel discs, are considered. The thermodynamic calculation of the rotor rod mount is investigated. An apparatus for testing the heat transfer characteristics of the rod mount rotor is designed and manufactured. The temperature field of the rod-mounted rotor is measured by the change in thrust force and roughness of the wheel surface. The results show that the heat transfer coefficient of the joint surface increases with increasing pre-tensioning of the rod and decreases with increasing roughness of the wheel surface. The results of a numerical study of the thermal stress-strain state of a rod under the action of laser beams are presented. The finite element method was used, presented in [7].

Based on the small parameter method, the paper [8] considers the problem of determining the stress-strain state of a rigid plastic pipe in the presence of temperature. The Mises contract was used. The work [9] provides an introduction to some of the best practices that have evolved in recent years in the field of nonlinear finite element modeling. This paper presents the instability of a material known as an adiabatic shear strip, which often occurs in a plastically deformable material when it undergoes rapid shear [10]. The work presents the basic principles of nonlinear continuum mechanics [11]. In [12], the temperature distribution inside the nuclear fuel rod is analyzed. This is necessary to prevent the release of dangerous fission products into the environment. For this purpose, the maximum fuel temperature must not exceed the fuel integrity limit. The fuel temperature distribution is obtained by calculating the heat transfer process inside the fuel rod. Multiple heat transfer processes with different heat transfer modes are interesting and important for nuclear fuel safety. This paper shows the applicability of CFD FLUENT and derives an analytical solution for calculating the temperature distribution inside a nuclear fuel rod.

In [13], the thermal characteristics of the laser are obtained by numerically solving the heat conduction equation. The temperature distributions in axial and radial directions in cylindrical coordinates are obtained. The thermal transient time in both directions as well as the thermal focal distance was calculated. The time behavior of the temperature distribution was illustrated in a three-dimensional diagram. It is noted in [14] that the microstructure of stainless and eutectoid steel changes during friction welding, resulting in changes in hardness and strength. In the paper, the non-stationary temperature distribution in a friction-welded joint was investigated. A numerical method based on thermal nets was used to estimate the transient temperature distribution. Changes in the microstructure of the specimen were also investigated. Preliminary predictions were compared with actual experimental data from welding carried out under identical conditions.

In [15], the basic computational relations of thermal force spatial bending with tension, transverse shear and torsion for a rod of rectangular cross-section consisting of different structural materials were obtained. The Timoshenko hypothesis was used. The obtained relations make it possible to perform approximate formulations and solutions of various direct and inverse problems, including determination of the stress-strain state of a rod component under the action of a thermal load, estimation of the strength and stiffness of a rod. This paper does not take into account the dependence of the thermal expansion coefficient and elastic modulus on the temperature of the rod, provided that it is pinched.

In [16], the thermal behavior of a bar during the hot rolling process was investigated using an offline hot rolling simulator and numerical simulation. In addition, it was compared with the sheet characteristics during the flat rolling process in order to understand the thermal behavior of the bar during the hot rolling process in more detail. The bar and sheet temperature during the hot rolling process was measured at several points with thermocouples using the rolling simulator, and then the measured temperature of each area of the billet was analyzed using numerical simulation.

The finite element method was used, presented in [17]. In [18], six types of Terfenol-D rods were developed to reduce the heating of the Terfenol-D rod and assess its efficiency. In doing so, the temperature field of the rods was modeled and calculated using the finite element method to obtain the temperature distribution. The results showed that the untreated rod had the highest temperature, with the temperature being higher in the middle and lower at both ends as well as on the surface of the outer diameter. The temperature distribution of the sliced rods was relatively more uniform. In [19], an unstable temperature distribution field in cylindrical rods subjected to laser heat sources was investigated. In these works, some values of the thermal-physical parameters of the rod are used as constants.

All this allows us to assert that it is expedient to conduct a study on developing a mathematical model of the thermomechanical state of a rod of variable cross-section, which takes into account the simultaneous effect of local temperature, thermal insulation and heat exchange with the environment.

3. The aim and objectives of the study

The aim of the study is to develop a method of accounting for the presence of local thermophysical processes in rods of variable cross-section. This will improve the reliability of elements of strategic equipment subjected to thermal stress.

To achieve the aim, the following objectives were set:

– to determine the temperature field within the length of each discrete element of a variable cross-section rod;

– to determine the stress and strain field;

– to determine the displacement field along the studied rod of variable cross-section.

4. Materials and methods

The investigated rod of variable cross-section and limited length is discretized by elements of length l=*L*/*n* (cm) [1, 2]. In this case, *n* is the number of discrete elements in the rod. Here l<<*L*. Consider the field of temperature distribution along the length of one discrete element l (cm), Fig. 1. The field of temperature distribution along the length of one discrete element is shown in Fig. 2.

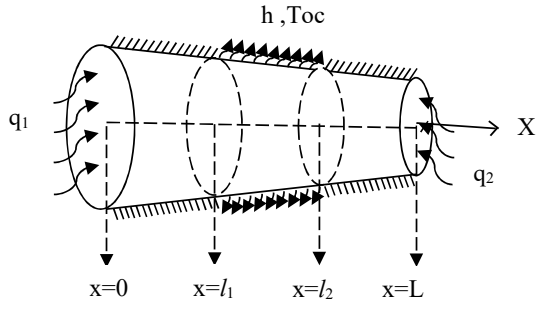

Fig. 1. Calculation scheme of the task

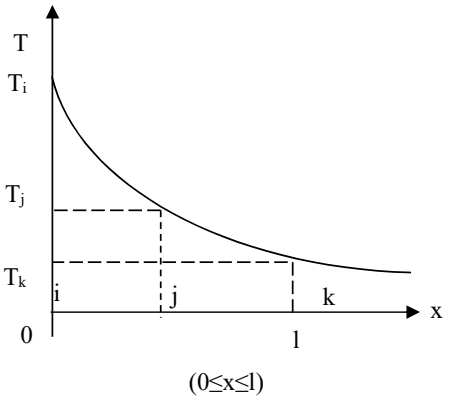

Fig. 2. Field of temperature distribution along the length of one discrete element

In the local coordinate system (0≤*x*≤l), the cross-section with the coordinate *x*=0 is denoted by *i*. Similarly, the cross-section with the coordinate *x*=l/2 is denoted by *j*. Finally, the cross-section with the coordinate *x*=l is denoted by *k*. The temperature values in the nodes *i*, *j*, *k* are denoted as T_i, T_j and T_k, respectively. The law of temperature distribution along the length of one discrete element is approximated by a complete polynomial of the second order, that is:

$$T(>C)=C_1x^2+C_2x+C_3,\ \ (0\le x\le l), \tag{1}$$

$$\varphi_i(x)=\begin{cases}1, x=0,\\ 0, x=\dfrac{l}{2},\\ 0, x=l;\end{cases}\ \ \varphi_j(x)=\begin{cases}0, x=0,\\ 1, x=\dfrac{l}{2},\\ 0, x=l;\end{cases}$$

$$\varphi_k(x)=\begin{cases}0, x=0,\\ 0, x=\dfrac{l}{2},\\ 1, x=l,\end{cases}$$

where C_1, C_2 and C_3 are constants.

With the above designations, the following system can be built to determine the values of constants C_1, C_2 and C_3:

$$\begin{cases}T(x=0)=C_1\cdot 0+C_2\cdot 0+C_3=T_i,\\ T\left(x=\dfrac{l}{2}\right)=C_1\cdot\dfrac{l^2}{4}+C_2\cdot\dfrac{l}{2}+C_3=T_j,\\ T(x=l)=C_1\cdot l^2+C_2\cdot l+C_3=T_k.\end{cases} \tag{2}$$

Thus, we find that:

$$C_3=T_i,\ \ C_2=\frac{4T_j-T_k-3T_i}{l},\ C_1=\frac{2}{l^2}\left(T_j-2T_k+T_i\right). \tag{3}$$

Further, substituting formula (3) in (1), we get:

$$T(x)=\frac{2x^2-3lx+l^2}{l^2}T_i+$$
$$+\frac{4lx-4x^2}{l^2}T_j+\frac{2x^2-lx}{l^2}T_k,\ \ (0\le x\le l). \tag{4}$$

Here we introduce the following designations:

$$\phi_i(x)=\frac{2x^2-3lx+l^2}{l^2};\ \ \phi_j(x)=\frac{4lx-4x^2}{l^2};$$

$$\phi_k(x)=\frac{2x^2-lx}{l^2};\ (0\le x\le l). \tag{5}$$

We call these functions quadratic spline functions in the local coordinate system (0≤*x*≤l). These functions have the following properties

$$\varphi_i(x)=\begin{cases}1, atx=0,\\ 0, atx=\dfrac{l}{2},\\ 0, atx=l;\end{cases}\ \ \varphi_j(x)=\begin{cases}0, atx=0,\\ 1, atx=\dfrac{l}{2},\\ 0, atx=l;\end{cases}$$

$$\varphi_k(x)=\begin{cases}0, atx=0,\\ 0, atx=\dfrac{l}{2},\\ 1, atx=l.\end{cases} \tag{6}$$

Also, it should be noted that

$$\phi_i(x)+\phi_j(x)+\phi_k(x)=1;\ \ \frac{\partial\phi_i}{\partial x}+\frac{\partial\phi_j}{\partial x}+\frac{\partial\phi_k}{\partial x}=0. \tag{7}$$

These properties of the quadratic spline functions provide the continuity of required functions upon transition from a discrete element to the next.

Using expressions (6), we rewrite (4) as follows:

$$T(x)=\phi_i(x)T_i+\phi_j(x)T_j+\phi_k(x)T_k,\ (0\le x\le l). \tag{8}$$

The expression of the temperature gradient within the length of one discrete element has the following form:

$$\frac{\partial T}{\partial x}=\frac{\partial\phi_i(x)}{\partial x}T_i+\frac{\partial\phi_j(x)}{\partial x}T_j+\frac{\partial\phi_k(x)}{\partial x}T_k=$$
$$=\frac{4x-3l}{l^2}T_i+\frac{4l-8x}{l^2}T_j+\frac{4x-l}{l^2}T_k,\qquad (0\le x\le l). \tag{9}$$

Similarly (8), the field of displacement within the length of one discrete element has the following form:

$$U(x)=\phi_i(x)U_i+\phi_j(x)U_j+\phi_k(x)U_k,\ (0\le x\le l), \qquad (10)$$

where U_i, U_j, U_k – the displacement of sections i, j, k.

5. Analysis of the results of the study of local surface heat exchange in rods of variable cross-section

5. 1. Determination of the temperature field in the rod of variable cross-section

Let us consider discrete elements of the studied rod of variable cross-section on the left to the right. First, we consider the first discrete element, starting from the left end of the rod (Fig. 3).

For this element, the functional of total thermal energy has the following form:

$$J_1=\int\limits_{F(x=0)} q_1T\mathrm{d}s+\int\limits_{V_1}\frac{K_{xx}}{2}\left(\frac{\partial T}{\partial x}\right)^2\mathrm{d}v,\ (0\le x\le l). \qquad (11)$$

For the first discrete element, local values i, j, k correspond to the global values of the nodes 1, 2 and 3.

Then, for the first discrete element of the studied core:

$$T_i=T_1;\ T_j=T_2;\ T_k=T_3.$$

Here the nodes 2 and 3 are internal. Now, taking into account physical laws, we integrate expression (11). For the first element of this expression, we have:

$$J_{11}=\int\limits_{F(x=0)} q_1T\mathrm{d}s=F(x=0)\cdot q_1T_i=\pi b_1^2q_1T_1, \qquad (12)$$

where $b_1=r(x=0)=a\cdot 0+b=b$.

Similarly, we consider the second integral on the volume of the first discrete element of the studied core:

$$\begin{aligned}
J_{12}&=\int\limits_{V_1}\frac{K_{xx}}{2}\left(\frac{\partial T}{\partial x}\right)^2\mathrm{d}v=\int\limits_0^l F(x)\left(\frac{\partial T}{\partial x}\right)^2\mathrm{d}x=\\
&=\int\limits_0^l\pi\left(a^2x^2+2ab_1x+b_1^2\right)\times\\
&\times\left[\left(\frac{4x-3l}{l^2}\right)T_1+\left(\frac{4l-8x}{l^2}\right)T_2+\left(\frac{4x-l}{l^2}\right)T_3\right]^2\mathrm{d}x=\\
&=\frac{\pi K_{xx}}{2}\left[\begin{array}{l}\left(\frac{a^2l}{5}+ab_1+\frac{7b_1^2}{3l}\right)T_1^2+\\ \left(\frac{32a^2l}{15}+\frac{16ab_1}{3}+\frac{16b_1^2}{3l}\right)T_2^2+\\ \left(\frac{23a^2l}{15}+\frac{11ab_1}{3}+\frac{7b_1^2}{3l}\right)T_3^2\end{array}\right]-\\
&-\left(\frac{4a^2l}{5}+\frac{8ab_1}{3}+\frac{16b_1^2}{3l}\right)T_1T_2+\\
&+\left(\frac{2a^2l}{5}+\frac{2ab_1}{3}+\frac{2b_1^2}{3l}\right)T_1T_3-\\
&-\left(\frac{52a^2l}{15}+8ab_1+\frac{16b_1^2}{3l}\right)T_2T_3. \qquad (13)
\end{aligned}$$

Here it is revealed that the sum of coefficients at T_1^2, T_2^2, T_3^2, T_1T_2, T_1T_3, T_2T_3 will be equal to zero.

Now we consider the second discrete element, through the side surfaces of which heat exchange with the environment occurs (Fig. 4).

The functional of total thermal energy for the second discrete element is as follows:

$$J_2=\int\limits_{V_2}\frac{K_{xx}}{2}\left(\frac{\partial T}{\partial x}\right)^2\mathrm{d}v+\int\limits_{S_{ass2}}\frac{h}{2}\left(T-T_{oc}\right)^2\mathrm{d}s,\ (0\le x\le l), \qquad (14)$$

where V_2 – the volume of the second discrete element, S_{ass2} – the area of the side surface of the second discrete element.

The integrated type of the functional J_2 has the following form:

$$\begin{aligned}
J_2=&\frac{\pi K_{xx}}{2}\left[\begin{array}{l}\left(\frac{a^2l}{5}+ab_2+\frac{7b_2^2}{3l}\right)T_3^2+\\ +\left(\frac{32a^2l}{15}+\frac{16ab_2}{3}+\frac{16b_2^2}{3l}\right)T_4^2+\\ +\left(\frac{23a^2l}{15}+\frac{11ab_2}{3}+\frac{7b_2^2}{3l}\right)T_5^2-\\ -\left(\frac{4a^2l}{5}+\frac{8ab_2}{3}+\frac{16b_2^2}{3l}\right)T_3T_4+\\ +\left(\frac{2a^2l}{5}+\frac{2ab_2}{3}+\frac{2b_2^2}{3l}\right)T_3T_5-\\ -\left(\frac{52a^2l}{15}+8ab_2+\frac{16b_2^2}{3l}\right)T_4T_5\end{array}\right]+\\
&+\pi h\left[\begin{array}{l}\left(\frac{a^2l}{60}+\frac{2b_2l}{15}\right)T_3^2+\left(\frac{4a\,l^2}{15}+\frac{8b_2l}{15}\right)T_4^2+\\ \left(\frac{7al^2}{60}+\frac{2b_2l}{15}\right)T_5^2+\\ \frac{2b_2l}{15}T_3T_4-\left(\frac{a\,l^2}{30}+\frac{b_2l}{15}\right)T_3T_5+\\ \left(\frac{2al^2}{15}+\frac{2b_2l}{15}\right)T_4T_5\end{array}\right]+\\
&+\pi h\left[\begin{array}{l}\left(\frac{al^2}{2}+b_2l\right)T_{oc}^2-\frac{b_2l}{3}T_3T_{oc}-\\ \left(\frac{2al^2}{3}+\frac{4b_2l}{3}\right)T_4T_{oc}-\left(\frac{al^2}{3}+\frac{b_2l}{3}\right)T_5T_{oc}\end{array}\right]. \qquad (15)
\end{aligned}$$

The sum of coefficients before nodal temperatures will be equal in this expression to zero.

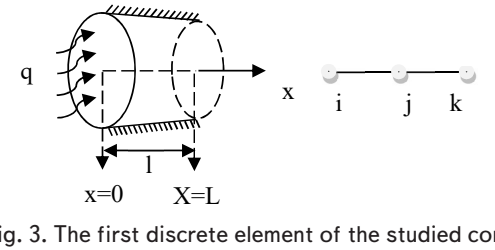

Fig. 3. The first discrete element of the studied core

Now we move on to the third discrete element. The side surface of this element is heat-insulated. On the cross-sec-

tional area of the left end, we bring a heat flux of intensity q_2 (Fig. 5).

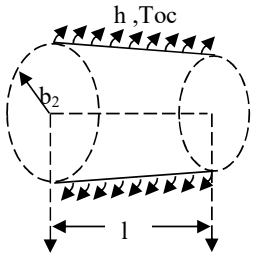

$b_2=al+b;$

Fig. 4. The second discrete element

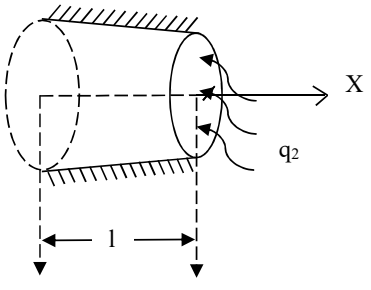

Fig. 5. The third discrete element

For the third discrete element, the functional of total thermal energy has the following form:

$$J_3=\int\limits_{V_3}\frac{K_{xx}}{2}\left(\frac{\partial T}{\partial x}\right)^2 \mathrm{d}v+\int\limits_{F(x=L)} q_2 T\mathrm{d}s,\ \left(0\le x\le l\right), \tag{16}$$

where V_3 – the volume of the third discrete element;

$F(x=L)$ – the cross-sectional area of the right end of the core $F(x=L)=F(x=3\mathrm{l})=\pi(al+b)^2=\pi(3al+b)^2$.

Then the integrated type of the functional J_3 has the following form:

$$J_3=\frac{\pi K_{xx}}{2}\left[\begin{array}{l}\left(\frac{a^2l}{5}+ab_3+\frac{7b_3^2}{3l}\right)T_5^2+\\+\left(\frac{32a^2l}{15}+\frac{16ab_3}{3}+\frac{16b_3^2}{3l}\right)T_6^2+\\+\left(\frac{23a^2l}{15}+\frac{11ab_3}{3}+\frac{7b_3^2}{3l}\right)T_7^2-\\-\left(\frac{4a^2l}{5}+\frac{8ab_3}{3}+\frac{16b_3^2}{3l}\right)T_5T_6+\\+\left(\frac{2a^2l}{5}+\frac{2ab_3}{3}+\frac{2b_3^2}{3l}\right)T_5T_7-\\-\left(\frac{52a^2l}{15}+8ab_3+\frac{16b_3^2}{3l}\right)T_6T_7\end{array}\right]+$$

$$+\pi\left(al+b\right)^2q_2T_7. \tag{17}$$

Then with the functional of total thermal energy for the studied core on nodal temperature values T_i, (i=1–7), we construct a system of linear algebraic equations taking into account natural boundary conditions

$$J=J_1+J_2+J_3. \tag{18}$$

Further, minimizing this functional on nodal temperature values T_i, (i=1–7), we construct a system of linear algebraic equations taking into account natural boundary conditions [9]:

$$1)\frac{\partial J}{\partial T_1}=0;\Rightarrow\frac{\pi K_{xx}}{2}\left[\begin{array}{l}\left(\frac{a^2l}{5}+ab_1+\frac{7b_1^2}{3l}\right)\cdot T_1-\\-\left(\frac{2a^2l}{5}+\frac{4ab_1}{3}+\frac{8b_1^2}{3l}\right)\cdot T_2+\\+\left(\frac{a^2l}{5}+\frac{ab_1}{3}+\frac{b_1^2}{3l}\right)\cdot T_3\end{array}\right]=$$

$$=-\pi b_1^2q_1;$$

$$2)\frac{\partial J}{\partial T_2}=0;\Rightarrow\pi K_{xx}\left[\begin{array}{l}\left(\frac{32a^2l}{15}+\frac{16ab_1}{3}+\frac{16b_1^2}{3l}\right)\cdot T_2-\\-\left(\frac{2a^2l}{5}+\frac{4ab_1}{3}+\frac{8b_1^2}{3l}\right)\cdot T_1-\\-\left(\frac{26a^2l}{15}+4ab_1+\frac{8b_1^2}{3l}\right)\cdot T_3\end{array}\right]=0;$$

$$3)\frac{\partial J}{\partial T_3}=0;\Rightarrow\pi K_{xx}\left[\begin{array}{l}\left(\frac{23a^2l}{5}+\frac{11ab_1}{3}+\frac{7b_1^2}{3l}\right)\cdot T_3+\\+\left(\frac{a^2l}{5}+\frac{ab_1}{3}+\frac{b_1^2}{3l}\right)\cdot T_1-\\-\left(\frac{26a^2l}{15}+8ab_1+\frac{16b_1^2)}{3l}\right)\cdot T_2+\\+\left(\frac{a^2l}{5}+ab_2+\frac{7b_2^2}{3l}\right)\cdot T_3-\\-\left(\frac{2a^2l}{5}+\frac{4ab_2}{3}+\frac{8b_2^2}{3l}\right)\cdot T_4+\\+\left(\frac{a^2l}{5}+\frac{ab_2}{3}+\frac{b_2^2}{3l}\right)\cdot T_5\end{array}\right]+$$

$$+\pi h\left[\begin{array}{l}2\cdot\left(\frac{a^2l}{60}+\frac{2b_2l}{15}\right)\cdot T_3+\frac{2b_2l}{15}\cdot T_4-\\-\left(\frac{al^2}{30}+\frac{b_2l}{15}\right)\cdot T_5-\frac{b_2l}{3}\cdot T_{oc}\end{array}\right]=0;$$

$$4)\frac{\partial J}{\partial T_4}=0;\Rightarrow\pi K_{xx}\left[\begin{array}{l}\left(\frac{32a^2l}{15}+\frac{16ab_2}{3}+\frac{16b_2^2}{3l}\right)\cdot T_4-\\-\left(\frac{2a^2l}{5}+\frac{4ab_2}{3}+\frac{8b_2^2}{3l}\right)\times\\\times T_3-\left(\frac{26a^2l}{15}+4ab_2+\frac{8b_2^2}{3l}\right)\cdot T_5\end{array}\right]+$$

$$+\pi h\left[\begin{array}{l}2\left(\frac{4al^2}{15}+\frac{8b_2l}{15}\right)\cdot T_4+\frac{2b_2l}{15}T_3+\\+\left(\frac{2al^2}{15}+\frac{2b_2l}{15}\right)\cdot T_5\\-\left(\frac{2al^2}{3}+\frac{4b_2l}{3}\right)\cdot T_{OC}\end{array}\right]=0;$$

$$5)\frac{\partial J}{\partial T_5}=0;\Rightarrow \pi K_{xx}\left[\begin{array}{l}\left(\frac{23a^2l}{15}+\frac{11ab_2}{3}+\frac{7b_2^2}{3l}\right)\cdot T_5+\\+\left(\frac{a^2l}{5}+\frac{ab_2}{3}+\frac{b_2^2}{3l}\right)\cdot T_3-\\-\left(\frac{26a^2l}{15}+4ab_2+\frac{8b_2^2}{3l}\right)\cdot T_4+\\+\left(\frac{a^2l}{5}+ab_3+\frac{7b_3^2}{3l}\right)\cdot T_5-\\-\left(\frac{2a^2l}{5}+\frac{4ab_2}{3}+\frac{8b_3^2}{3l}\right)\cdot T_6+\\+\left(\frac{a^2l}{5}+\frac{ab_3}{3}+\frac{6b_3^2}{3l}\right)\cdot T_7\end{array}\right]+$$

$$+\pi h\left[\begin{array}{l}2\cdot\left(\frac{7al^2}{60}+\frac{2b_2l}{15}\right)\cdot T_5-\left(\frac{al^2}{30}+\frac{b_2l}{15}\right)\cdot T_3+\\+\left(\frac{2al^2}{15}+\frac{2b_2l}{15}\right)\cdot T_4-\left(\frac{al^2}{3}+\frac{b_2l}{3}\right)\cdot T_{oc}\end{array}\right]=0; \quad (19)$$

$$6)\frac{\partial J}{\partial T_6}=0;\Rightarrow K_{xx}\left[\begin{array}{l}\left(\frac{32a^2l}{15}+\frac{16ab_3}{3}+\frac{16b_3^2}{3l}\right)\cdot T_6-\\-\left(\frac{2a^2l}{5}+\frac{4ab_3}{3}+\frac{8b_3^2}{3l}\right)\cdot T_5-\\-\left(\frac{26a^2l}{15}+4ab_3+\frac{8b_3^2}{3l}\right)\cdot T_7\end{array}\right]=0;$$

$$7)\frac{\partial J}{\partial T_7}=0;\Rightarrow \pi K_{xx}\left[\begin{array}{l}\left(\frac{23a^2l}{15}+\frac{11ab_3}{3}+\frac{7b_3^2}{3l}\right)\cdot T_7+\\+\left(\frac{a^2l}{5}+\frac{ab_3}{3}+\frac{b_3^2}{3l}\right)\cdot T_5-\\-\left(\frac{26a^2l}{15}+4ab_3+\frac{8b_3^2}{3l}\right)\cdot T_6\end{array}\right]=$$

$$=-\pi(aL+b)^2\cdot q_2.$$

Solving this system, the nodal temperature values T_i, (i=1–7) are defined. According to them, the law of temperature distribution along the length of the studied core is constructed as follows:

– for the first site of the core:

$$T(x)=\phi_i(x)T_1+\phi_j(x)T_2+\phi_k(x)T_3,\ (0\le x\le l). \quad (20)$$

– for the second site of the core:

$$T(x)=\phi_i(x)T_3+\phi_j(x)T_4+\phi_k(x)T_5,\ (0\le x\le l). \quad (21)$$

Finally, for the third site of the core we have:

$$T(x)=\phi_i(x)T_5+\phi_j(x)T_6+\phi_k(x)T_7,\ (0\le x\le l). \quad (22)$$

Using these formulas, it is possible to obtain a field of temperature distribution over the entire length of the rod of variable cross-section.

To illustrate the above method and a computing algorithm, we consider the problem with the following input data:

$$L=30\text{ cm};\ \ l=\frac{L}{3}=10\text{ cm};\ \ a=-\frac{1}{30};$$

$$b=2\text{ cm};\ \ b_2=\frac{5}{3}\text{cm};\ \ b_3=\frac{4}{3}\text{cm};$$

$$K_{xx}=100\frac{\text{W}}{\text{cm}^\circ\text{C}};\ \ \alpha=125\cdot10^{(-7)}\frac{1}{^\circ\text{C}};\ \ E=2\cdot10^6\frac{\text{kG}^2}{\text{cm}^2};$$

$$q_1=q_2=-500\frac{\text{W}}{\text{cm}^2};\quad h=10\frac{\text{W}}{\text{cm}^2{}^\circ\text{C}};\quad T_{oc}=30\,^\circ\text{C}.$$

These input data show that the studied core is sampled by three discrete elements of identical length. At the same time, lateral areas of the first and third discrete elements are completely heat-insulated. In this case, heat exchange with the environment occurs through the lateral area of the second element. On the cross-sectional area of the two ends of the core, heat fluxes of identical intensity are brought.

Fig. 6 shows the law of temperature distribution along the length of the studied rod of variable cross-section. The temperature value at the left end of the rod is T (x=0)=112.06 °C. At the same time, at the right end, T (x=30 cm)=75.69 °C. This difference is motivated by the fact that the cross-sectional area of the left end F (x=0)=4π cm^2, and the area at the right end F (x=30 cm)=π cm^2. Thus, F (x=0)/F (x=30 cm)=4. This means that at the left end, $q\cdot F$ (x=0)=–500·4π=–2,000·π (w). While $q\cdot F$ (x=30 cm)=–500·π (w). Therefore, the temperature value at the left end exceeds 1.49 times the temperature value at the right end of the investigated rod of variable cross-section. Due to the heat exchange of the middle part of 1/3 of the rod with the environment, the temperature value in the cross-section with the coordinate x=16.87 cm will be minimal, that is, T (x=16.87 cm)=34.238 °C.

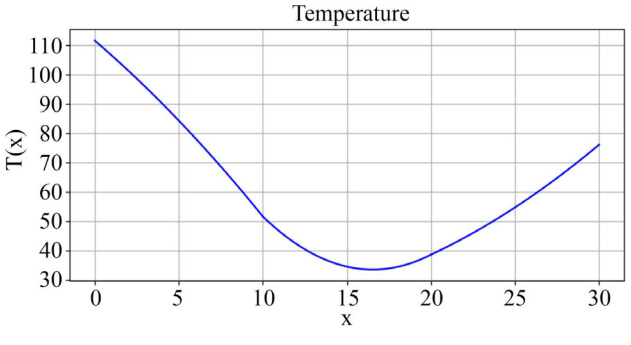

Fig. 6. Temperature dependency T

5. 2. Definition of the stress and strain field

If one end of the considered horizontally located rod of variable cross-section is rigidly jammed, then it is extended due to the temperature field. The value of lengthening is defined by the general laws of thermophysics:

$$\Delta l_T=\int_0^L\alpha T(x)\,dx, \quad (23)$$

where α[1/°K] – the coefficient of thermal expansion of the core material. $T(x)$ is the law of temperature distribution along the core length. If we accept that α=const, then the value of lengthening for the studied core is defined as follows:

$$\Delta l_T = \int_0^L \alpha T(x)dx =$$
$$= \alpha \begin{bmatrix} \int_0^l \left[\varphi_i(x)T_1 + \varphi_j(x)T_2 + \varphi_k(x)T_3\right]dx + \\ \int_0^l \left[\varphi_i(x)T_3 + \varphi_j(x)T_4 + \varphi_k(x)T_5\right]dx + \\ \int_0^l \left[\varphi_i(x)T_5 + \varphi_j(x)T_6 + \varphi_k(x)T_7\right]dx \end{bmatrix} =$$
$$= \alpha\left[\frac{l}{6}T_1 + \frac{2l}{3}T_2 + \frac{l}{3}T_3 + \frac{2l}{3}T_4 + \frac{l}{3}T_5 + \frac{2l}{3}T_6 + \frac{l}{6}T_7\right] =$$
$$= \frac{\alpha l}{6}\left[T_1 + 4T_2 + 2T_3 + 4T_4 + 2T_5 + 4T_6 + T_7\right]; \quad (24)$$

$$\varepsilon_T(x) = -\alpha T(x) == -\frac{\alpha}{l^2} \times$$
$$\times \begin{bmatrix} \left(2x^2 - 3lx + l^2\right)T_1 + \left(4lx - 4x^2\right)T_2 + \\ \left(4x^2 - 4lx + l^2\right)T_3 + \left(4lx - 4x^2\right)T_4 + \\ \left(4x^2 - 4lx + l^2\right)T_5 + \left(4lx - 4x^2\right)T_6 + \\ \left(2x^2 - lx\right)T_7 \end{bmatrix}, \ (0 \le x \le l). \quad (25)$$

If both ends of the studied core are rigidly jammed, then a thermo-intensely strain state occurs in it, and also an axial compressive force R (kg).

In case of jamming of two ends of the studied core, it is not extended and does not shorten. But there is an axial compressive force R (Fig. 7).

To determine the magnitude of the resulting axial force R, we find the average cross-sectional area:

$$F_{cp} = \frac{\int_0^L F(x)\mathrm{d}x}{L} = \frac{\int_0^L \left(a^2x^2 + 2abx + b^2\right)\mathrm{d}x}{L} =$$
$$= \left(\frac{a^2L^2}{3} + abL + b^2\right), \quad (26)$$

where F_{cp} (cm^2).

Let us consider the problem of compression of the studied core under the influence of the axial force R (Fig. 8).

In this case, the core is shortened by Δl_R. It is defined proceeding from the general Hooke's law:

$$\Delta l_R = \frac{RL}{EF_{cp}}. \quad (27)$$

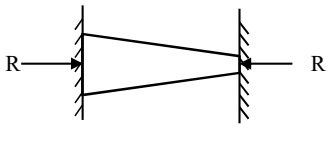

Fig. 7. Rod of variable cross-section under the influence of an axial compressive force R

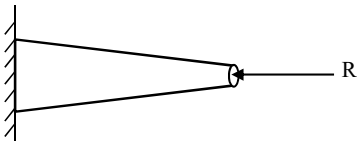

Fig. 8. Compression of a rod of variable cross-section by the axial force R

In case of jamming of two ends of the studied rod of variable cross-section, it can be extended and shortened. Then we have:

$$\Delta l_T + \Delta l_R = 0. \quad (28)$$

Substituting (25), (27) in (28), we find the magnitude of the arising axial force:

$$R = -\frac{EF_{cp}}{L}\Delta l_T =$$
$$= -\frac{\alpha EF_{cp}l}{6L}\left(T_1 + 4T_2 + 2T_3 + 4T_4 + 2T_5 + 4T_6 + T_7\right). \quad (29)$$

Then, in this case, there is a distribution field of the thermoelastic stress component along the length of the studied core:

$$\sigma_T(x) = \frac{R}{F(x)} = -\frac{\alpha EF_{cp}l}{6L\pi\left(a^2x^2 + 2abx + b^2\right)} \times$$
$$\times\left(T_1 + 4T_2 + 2T_3 + 4T_4 + 2T_5 + 4T_6 + T_7\right),$$
$$(0 \le x \le l). \quad (30)$$

The distribution law of the thermoelastic strain component ε is also defined by $T(x)$ on the basis of the corresponding Hooke's law:

$$\varepsilon(x) = \frac{\sigma(x)}{E} =$$
$$= -\frac{\alpha F_{cp}l}{6L\pi\left(a^2x^2 + 2abx + b^2\right)} \times$$
$$\times\left(T_1 + 4T_2 + 2T_3 + 4T_4 + 2T_5 + 4T_6 + T_7\right), \ (0 \le x \le l). \quad (31)$$

In case of jamming of two ends of the studied rod of variable cross-section, there is also a field of distribution of the temperature strain component ε_T (x) along its length. It is defined on the basis of fundamental laws of thermophysics:

$$\varepsilon_T(x) = -\alpha T(x) =$$
$$= -\frac{\alpha}{l^2}\begin{bmatrix} \left(2x^2 - 3lx + l^2\right)T_1 + \left(4lx - 4x^2\right)T_2 + \\ + \left(4x^2 - 4lx + l^2\right)T_3 + \\ + \left(4lx - 4x^2\right)T_4 + \left(4x^2 - 4lx + l^2\right)T_5 + \\ + \left(4lx - 4x^2\right)T_6 + \left(2x^2 - lx\right)T_7 \end{bmatrix}. \quad (32)$$

Then also in compliance with the generalized Hooke's law, the distribution law of the temperature stress component along the studied rod of variable cross-section is defined:

$$\sigma_T(x) = E\varepsilon_T(x) =$$
$$= -\frac{\alpha E}{l^2}\begin{bmatrix} \left(2x^2 - 3lx + l^2\right)T_1 + \left(4lx - 4x^2\right)T_2 + \\ + \left(4x^2 - 4lx + l^2\right)T_3 + \left(4lx - 4x^2\right)T_4 + \\ + \left(4x^2 - 4lx + l^2\right)T_5 + \left(4lx - 4x^2\right)T_6 + \\ + \left(2x^2 - lx\right)T_7 \end{bmatrix}. \quad (33)$$

The distribution field of the elastic strain component $\varepsilon_x(x)$ is defined on the basis of the theory of thermoelasticity:

$$\varepsilon_x(x)=\varepsilon(x)-\varepsilon_T(x)=$$
$$=-\frac{\alpha F_{cp} l}{6L\pi\left(a^2x^2+2abx+b^2\right)}\begin{pmatrix}T_1+4T_2+\\+2T_3+4T_4+\\+2T_5+4T_6+T_7\end{pmatrix}+$$
$$+\frac{\alpha}{l^2}\begin{bmatrix}\left(2x^2-3lx+l^2\right)T_1+\left(4lx-4x^2\right)T_2+\\+\left(4x^2-4lx+l^2\right)T_3+\left(4lx-4x^2\right)T_4+\\+\left(4x^2-4lx+l^2\right)T_5+\left(4lx-4x^2\right)T_6+\\+\left(2x^2-lx\right)T_7\end{bmatrix}. \quad (34)$$

$$\sigma_x(x)=\sigma(x)-\sigma_T(x)=-\frac{\left(\alpha EF_{cp} l\right)}{6L^2\left(a^2x^2+2abx+b^2\right)}+$$
$$+\frac{\alpha E}{l^2}\begin{bmatrix}\left(2x^2-3lx+l^2\right)T_1+\\+\left(4lx-4x^2\right)T_2+\\+\left(4x^2-4lx+l^2\right)T_3+\\+\left(4lx-4x^2\right)T_4+\left(4x^2-4lx+l^2\right)T_5+\\+\left(4lx-4x^2\right)T_6+\left(2x^2-lx\right)T_7\end{bmatrix}. \quad (35)$$

In compliance with Hooke's law, from (33) it is possible to define the distribution law of the elastic stress component (35) along the studied rod of variable cross-section.

Fig. 9 shows distribution laws for the three strain components. Here curve 1 is the distribution law of the thermo-elastic strain component. It has a compressive nonlinear character along the entire length of the rod.

Fig. 10 shows the distribution law for the thermo-elastic $\sigma(x)$ and $\sigma_T(x)$ and elastic $\sigma_x(x)$ components along the length of the studied rod of variable cross-section.

In addition, this is due to the fact that the radius of the cross-section of the rod from the left to the right. If the left end of the rod is rigidly clamped, and the right end is free, then the investigated rod of variable cross-section is extended. The magnitude of elongation with the obtained initial data is

$$\Delta l_T=\int_0^L \alpha T(x)\mathrm{d}x=0.02214 \text{ cm}.$$

If both ends of the rod are rigidly clamped, then it cannot be extended. In this case, due to the thermal expansion of the material, an axial compressive force R (kg) arises. With our initial data, the value of this force will be R=–10820.8148 kg.

5. 3. Determination of the displacement field along the studied rod of variable cross-section

We approximate the field of displacement distribution along one discrete element in the local coordinate system by quadratic spline functions:

$$U(x)=\phi_i(x)U_i+\phi_j(x)U_j+\phi_k(x)U_k=$$
$$=\frac{2x^2-3lx+l^2}{l^2}U_i+\frac{4lx-4x^2}{l^2}U_j+\frac{2x^2-lx}{l^2}U_k,$$
$$\left(0\le x\le l\right), \quad (36)$$

where in the local coordinate system U_i=$U(x$=0); U_i=$U(x$=l/2); U_i=$U(x$=l).

Then in this local coordinate system, the distribution law of the elastic strain component $\varepsilon_x(x)$ is defined by the Cauchy relation:

$$\varepsilon_x(x)=\frac{\partial U}{\partial x}=\frac{4x-3l}{l^2}U_i+\frac{4l-8x}{l^2}U_j+\frac{4x-l}{l^2}U_k,$$
$$\left(0\le x\le l\right). \quad (37)$$

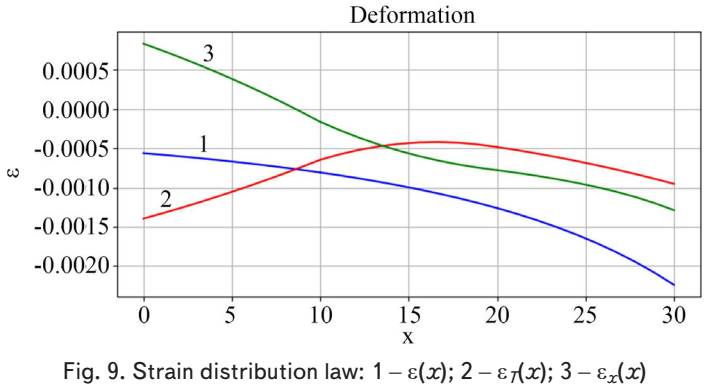

Fig. 9. Strain distribution law: 1 – $\varepsilon(x)$; 2 – $\varepsilon_T(x)$; 3 – $\varepsilon_x(x)$

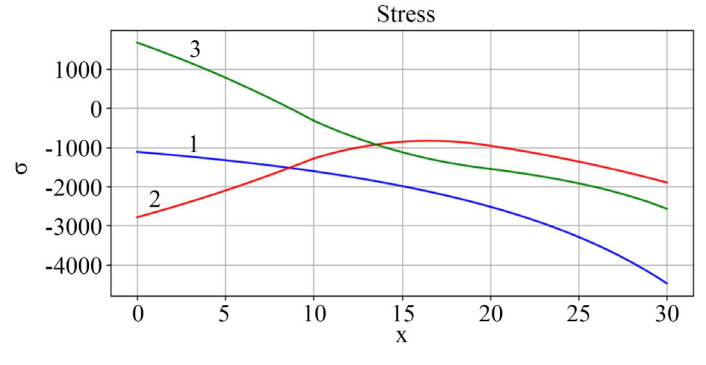

Fig. 10. Stress distribution law: 1 – $\sigma(x)$; 2 – $\sigma_T(x)$; 3 – $\sigma_x(x)$

On the other hand, the functional of potential elastic strain energy in the local coordinate system for the studied rod of variable cross-section has the following form:

$$\Pi=\int_V\frac{\sigma_x}{2}\varepsilon_x\mathrm{d}V-\int_V\alpha ET(x)\varepsilon_x\mathrm{d}V=\int_V\frac{E\varepsilon_x}{2}\varepsilon_x\mathrm{d}V-\int_V\alpha ET(x)\varepsilon_x\mathrm{d}V=$$

$$=\frac{E}{2}\int_V{\varepsilon_x}^2\mathrm{d}V-\alpha E\int_V T(x)\varepsilon_x\mathrm{d}V\frac{E}{2}\int_V\left(\frac{\partial U}{\partial x}\right)^2\mathrm{d}V-\alpha E\int_V T(x)\frac{\partial U}{\partial x}\mathrm{d}V=$$

$$=\frac{E\pi}{2}\left\{\begin{array}{l}\int_0^l\left(a^2x^2+2abx+b^2\right)\left[\frac{4x-3l}{l^2}U_1+\frac{4l-8x}{l^2}U_2+\frac{4x-l}{l^2}U_3\right]^2\mathrm{d}x+\\+\int_0^l\left(a^2x^2+2ab_2x+{b_2}^2\right)\left[\frac{4x-3l}{l^2}U_3+\frac{4l-8x}{l^2}U_4+\frac{4x-l}{l^2}U_5\right]^2\mathrm{d}x+\\+\int_0^l\left(a^2x^2+2ab_3x+{b_3}^2\right)\left[\frac{4x-3l}{l^2}U_5+\frac{4l-8x}{l^2}U_6+\frac{4x-l}{l^2}U_7\right]^2\mathrm{d}x\end{array}\right\}-$$

$$-\alpha E\left\{\begin{array}{l}\int_0^l\left[\left(\frac{2x^2-3lx+l^2}{l^2}\right)T_1+\left(\frac{4lx-4x^2}{l^2}\right)T_2+\left(\frac{2x^2-lx}{l^2}\right)T_3\right]\times\\\times\left[\frac{4x-3l}{l^2}U_1+\frac{4l-8x}{l^2}U_2+\frac{4x-l}{l^2}U_3\right]\mathrm{d}x+\\+\int_0^l\left[\left(\frac{2x^2-3lx+l^2}{l^2}\right)T_3+\left(\frac{4lx-4x^2}{l^2}\right)T_4+\left(\frac{2x^2-lx}{l^2}\right)T_5\right]\times\\\times\left[\frac{4x-3l}{l^2}U_3+\frac{4l-8x}{l^2}U_4+\frac{4x-l}{l^2}U_5\right]\mathrm{d}x+\\+\int_0^l\left[\left(\frac{2x^2-3lx+l^2}{l^2}\right)T_5+\left(\frac{4lx-4x^2}{l^2}\right)T_6+\left(\frac{2x^2-lx}{l^2}\right)T_7\right]\times\\\times\left[\frac{4x-3l}{l^2}U_5+\frac{4l-8x}{l^2}U_6+\frac{4x-l}{l^2}U_7\right]\mathrm{d}x\end{array}\right\}=$$

$$=\frac{E\pi}{2}\left[\begin{array}{l}\left(\begin{array}{l}\frac{a^2l}{5}U_1^2+abU_1^2+\frac{7b^2}{3l}U_1^2-\frac{4a^2l}{5}U_1U_2-\frac{8ab}{3}U_1U_2-\\-\frac{16b^2}{3l}U_1U_2+\frac{2a^2l}{5}U_1U_3+\frac{2ab}{3}U_1U_3+\frac{2b^2}{3l}U_1U_3+\\+\frac{32a^2l}{5}U_2^2+\frac{16ab}{3}U_2^2+\frac{16b^2}{3l}U_2^2-\frac{52a^2l}{15}U_2U_3-\\-8abU_2U_3-\frac{16ab^2}{3}U_2U_3+\frac{23a^2l}{15}U_3^2+\frac{11ab}{3}U_3^2+\frac{7b^2}{3l}U_3^2\end{array}\right)+\\+\left(\begin{array}{l}\frac{a^2l}{5}U_3^2+abU_3^2+\frac{7b^2}{3l}U_3^2-\frac{4a^2l}{5}U_3U_4-\frac{8ab}{3}U_3U_4-\\-\frac{16b^2}{3l}U_3U_4+\frac{2a^2l}{5}U_3U_4+\frac{2ab}{3}U_3U_4+\frac{2b^2}{3l}U_3U_4+\\+\frac{32a^2l}{5}U_4^2+\frac{16ab}{3}U_4^2+\frac{16b^2}{3l}U_4^2-\frac{52a^2l}{15}U_4U_5-\\-8abU_4U_5-\frac{16ab^2}{3}U_4U_5+\frac{23a^2l}{15}U_5^2+\frac{11ab}{3}U_5^2+\frac{7b^2}{3l}U_5^2\end{array}\right)+\\+\left(\begin{array}{l}\frac{a^2l}{5}U_5^2+abU_5^2+\frac{7b^2}{3l}U_5^2-\frac{4a^2l}{5}U_5U_6-\frac{8ab}{3}U_5U_6-\\-\frac{16b^2}{3l}U_5U_6+\frac{2a^2l}{5}U_5U_7+\frac{2ab}{3}U_5U_7+\frac{2b^2}{3l}U_5U_7+\\+\frac{32a^2l}{5}U_6^2+\frac{16ab}{3}U_6^2+\frac{16b^2}{3l}U_6^2-\frac{52a^2l}{15}U_6U_7-\\-8abU_6U_7-\frac{16ab^2}{3}U_6U_7+\frac{23a^2l}{15}U_7^2+\frac{11ab}{3}U_7^2+\frac{7b^2}{3l}U_7^2\end{array}\right)\end{array}\right]-$$

$$-\alpha E\left[\begin{array}{l}\left(\begin{array}{l}-\frac{1}{2}T_1U_1+\frac{2}{3}T_1U_2-\frac{1}{6}T_1U_3-\\-\frac{2}{3}T_2U_1+\frac{2}{3}T_2U_3+\frac{1}{6}T_3U_1-\\-\frac{2}{3}T_3U_2-\frac{1}{2}T_3U_3\end{array}\right)+\left(\begin{array}{l}-\frac{1}{2}T_3U_3+\frac{2}{3}T_3U_5-\frac{1}{6}T_3U_5-\\-\frac{2}{3}T_4U_3+\frac{2}{3}T_4U_5+\frac{1}{6}T_5U_3-\\-\frac{2}{3}T_5U_4-\frac{1}{2}T_5U_5\end{array}\right)+\\+\left(\begin{array}{l}-\frac{1}{2}T_5U_5+\frac{2}{3}T_5U_6-\frac{1}{6}T_5U_7-\frac{2}{3}T_6U_5+\\+\frac{2}{3}T_6U_7+\frac{1}{6}T_7U_5-\frac{2}{3}T_7U_6-\frac{1}{2}T_7U_7\end{array}\right)\end{array}\right].$$

If both ends of the studied core are rigidly jammed, then $U_1=U_7=0$. Then it will be necessary to define the values of U_2, U_3, U_4, U_5 and U_6. Minimizing the functional of potential elastic strain energy on these nodal displacement values, we construct a system of simple algebraic equations taking into account natural boundary conditions:

$$\left\{\begin{array}{l}\frac{\partial\mathrm{P}}{\partial U_2}=0;\Rightarrow\frac{E\pi}{2}\left[\begin{array}{l}\frac{64a^2l}{15}U_2+\frac{32ab}{3}U_2+\frac{32b^2}{3l}U_2\\-\frac{52a^2l}{15}U_3-8abU_3-\frac{16b^2}{3l}U_3\end{array}\right]-\\-\alpha E\left[\left(\frac{2}{3}T_1-\frac{2}{3}T_3\right)\right]=0;\\\frac{\partial\mathrm{P}}{\partial U_3}=0;\Rightarrow\frac{E\pi}{2}\left[\begin{array}{l}\left(\begin{array}{l}-\frac{52a^2l}{15}U_2-8abU_2-\frac{16b^2}{3l}U_2+\\\frac{46a^2l}{15}U_3+\frac{22ab}{3}U_3+\frac{14b^2}{3l}U_3\end{array}\right)+\\+\left(\begin{array}{l}\frac{2a^2l}{5}U_3+2ab_2U_3+\frac{14{b_2}^2}{3l}U_3\\-\frac{4a^2l}{5}U_4-\frac{8ab_2}{3}U_4+\frac{16{b_2}^2}{3l}U_4+\\\frac{2a^2l}{5}U_5+\frac{2ab_2}{3}U_5+\frac{2{b_2}^2}{3l}U_5\end{array}\right)\end{array}\right]-\\-\alpha E\left[\left(-\frac{1}{6}T_1+\frac{2}{3}T_2+\frac{1}{3}T_3-\frac{1}{3}T_3-\frac{2}{3}T_4+\frac{1}{6}T_5\right)\right]=0;\\\frac{\partial\mathrm{P}}{\partial U_4}=0;\Rightarrow\frac{E\pi}{2}\left[\begin{array}{l}\left(\begin{array}{l}-\frac{4a^2l}{5}U_3-\frac{8ab_2}{3}U_3-\frac{16{b_2}^2}{3l}U_3+\\+\frac{64a^2l}{15}U_4+\frac{32ab_2}{3}U_4+\frac{32{b_2}^2}{3l}U_4\end{array}\right)+\\-\frac{52a^2l}{15}U_5-8ab_2U_5-\frac{16{b_2}^2}{3l}U_5\end{array}\right]-\\-\alpha E\left[-\frac{2}{3}T_5+\frac{2}{3}T_3\right]=0;\\\frac{\partial\mathrm{P}}{\partial U_5}=0;\Rightarrow\frac{E\pi}{2}\left[\begin{array}{l}\left(\begin{array}{l}\frac{2a^2l}{5}U_3+\frac{2ab_2}{3}U_3+\frac{2{b_2}^2}{3l}U_3-\\-\frac{52a^2l}{15}U_4-8ab_2U_4-\\-\frac{16{b_2}^2}{3l}U_4+\frac{46a^2l}{15}U_5+\\+\frac{22ab_2}{3}U_5+\frac{14{b_2}^2}{3l}U_5\end{array}\right)+\\\left(\begin{array}{l}\frac{2a^2l}{5}U_5+2ab_3U_5+\frac{14{b_3}^2}{3l}U_5-\\\frac{4a^2l}{5}U_6-\frac{8ab_3}{3}U_6-\frac{16{b_3}^2}{3l}U_6\end{array}\right)\end{array}\right]-\\-\alpha E\left[\left(-\frac{1}{6}T_3+\frac{2}{3}T_4+\frac{1}{2}T_5\right)+\left(-\frac{1}{2}T_5-\frac{2}{3}T_6+\frac{1}{6}T_7\right)\right]=0;\\\frac{\partial\mathrm{P}}{\partial U_6}=0;\Rightarrow\frac{E\pi}{2}\left[\begin{array}{l}-\frac{4a^2l}{5}U_5-\frac{8ab_3}{3}U_5-\frac{16{b_3}^2}{3l}U_5+\\\frac{64a^2l}{15}U_6+\frac{32ab_3}{3}U_6+\frac{32{b_3}^2}{3l}U_6\end{array}\right]-\\-\alpha E\left[\frac{2}{3}T_5-\frac{2}{3}T_7\right]=0;\end{array}\right.\qquad(38)$$

After simplification, we get:

$$\begin{cases} \frac{E\pi}{2}\left[\frac{192a^2l^2+160abl+160b^2}{15l}U_2-\frac{52a^2l^2+120abl+80b^2}{15l}U_3\right]- \\ -\frac{2}{3}\alpha E\left[T_1-T_3\right]=0; \\ \frac{E\pi}{2}\left[\begin{array}{l}\frac{-52a^2l^2-120abl-80b^2}{15l}U_2+ \\ +\frac{52a^2l^2+110abl+70b^2+30ab_2l+70b_2^2}{15l}U_3- \\ -\frac{12a^2l^2+40ab_2l+80b_2^2}{15l}U_4+ \\ +\frac{6a^2l^2+10ab_2l+10b_2^2}{15l}U_5\end{array}\right]+ \\ +\frac{\alpha E}{6}\left[T_1-4T_2+4T_4-T_5\right]=0; \\ \frac{E\pi}{2}\left[\begin{array}{l}\frac{-12a^2l^2-40ab_2l-80b_2^2}{15l}U_3+ \\ +\frac{64a^2l^2+160ab_2l+160b_2^2}{15l}U_4- \\ -\frac{52a^2l^2+120ab_2l+80b_2^2}{15l}U_5\end{array}\right]- \\ -\frac{2\alpha E}{3}\left[T_3-T_5\right]=0; \\ \frac{E\pi}{2}\left[\begin{array}{l}\frac{6a^2l^2+10ab_2l+10b_2^2}{15l}U_3- \\ -\frac{52a^2l^2+120ab_2l+80b_2^2}{15l}U_4+ \\ +\frac{52a^2l^2+110ab_2l+70b_2^2+30ab_3l+70b_3^2}{15l}U_5- \\ -\frac{12a^2l^2+40ab_3l+80b_3^2}{15l}U_6\end{array}\right]+ \\ +\frac{\alpha E}{6}\left[T_3-4T_4+4T_6-T_7\right]=0; \\ \frac{E\pi}{2}\left[\begin{array}{l}\frac{-12a^2l^2-40ab_3l-80b_3^2}{15l}U_5+ \\ +\frac{64a^2l^2+160ab_3l+160b_3^2}{15l}U_6\end{array}\right]-\frac{2\alpha E}{3}\left[T_5-T_7\right]=0. \end{cases} \quad (39)$$

Solving this system, we define the values of nodal displacements. The distribution law of displacement of the core sections is determined by them. Along the 1st site of the core, the law of displacement distribution is determined by the formula:

$$U^I(x)=\frac{4lx-4x^2}{l^2}U_2+\frac{2x^2-lx}{l^2}U_3;\ \ (0\le x\le l). \quad (40)$$

On the second site of the core ($l\le x\le 2l$), the law of displacement distribution is defined as follows:

$$U^{II}(x)=\frac{2x^2-3lx+l^2}{l^2}U_3+ \\ +\frac{4lx-4x^2}{l^2}U_4+\frac{2x^2-lx}{l^2}U_5;\ \ (0\le x\le l). \quad (41)$$

The law of displacement distribution on the last third site of the core is determined by the formula:

$$U^{III}(x)=\frac{2x^2-3lx+l^2}{l^2}U_5+\frac{4lx-4x^2}{l^2}U_6;\ \ (0\le x\le l). \quad (42)$$

The formulas (40)–(42) determine the law of displacement along the length of the rod of variable cross-section.

Fig. 11 shows the displacement field. For this, a system of resolving equations was solved with respect to nodal displacement values (39). As a result, U_i (i=1–7) was obtained. Further, using the formula (36), the field of displacement along the length of each discrete element is determined.

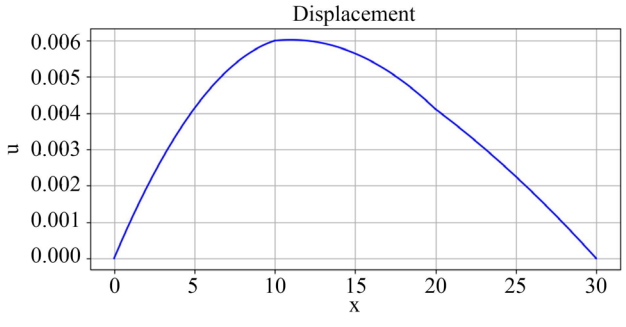

Fig. 11. Dependences of displacement along the length of the rod

6. Discussion of the results of the study of local surface heat exchange in rods of variable cross-section

Fig. 6 shows the law of temperature distribution along the length of the rod in question. First, we determine nodal temperature values using the obtained resolving equations taking into account natural boundary conditions (19). As a result, the nodal temperature values T_i (i=1–7) are obtained. Then, using formula (4), the temperature distribution field is determined within the length of each discrete element.

Fig. 9 shows the distribution fields of three strain components:

1) $\varepsilon(x)$ – the distribution field of thermoelastic strain, determined by formula (31);

2) $\varepsilon_x(x)$ – the distribution field of the elastic strain component, determined by formula (34);

3) $\varepsilon_T(x)$ – the distribution field of the temperature strain component, determined by formula (32).

Then, in this case, a steady thermo-stress-strain state arises in the rod.

The value is $\varepsilon(x=0)=-0.00043$, $\varepsilon(x=30\text{ cm})=-0.001722$. This means that the value $\varepsilon(x)$ at the left end of the rod is 4 times less than at the right. This process is due to the fact that the cross-sectional area of the left end of the rod is 4 times larger than the right one. The law of distribution of the temperature component $\varepsilon_T(x)$ along the entire length of the studied rod of variable cross-section has a compressive and non-linear character. Moreover, its maximum value $\varepsilon_T(x)=-0.0014$ is observed at the left end of the rod. There is a monotonous reduction of $\varepsilon_T(x)$ to the cross-section of the rod, the coordinate of which is x=16.25 cm. Here $\varepsilon_T(x=16.25)=-0.00042854$. This is due to heat exchange through the side surface of the middle section of the rod with

the environment. Then again, $\varepsilon_T(x)$ has a slightly increasing nature, and $\varepsilon_T(x=30\text{ cm})=-0.000964619$. In the distribution law of $\varepsilon_T(x)$, it is revealed that:

$$\varepsilon_T(x=0)/\varepsilon_T(x=L=30\text{ cm})=1.4804.$$

This is due to the fact that the cross-sectional area of the left end of the studied rod is 4 times larger than the right. In contrast to other laws, the distribution of the elastic strain component along the length of the studied rod of variable cross-section has a sign-variable character. In particular $\varepsilon_x(x)$, in the area of the $0\leq x\leq 10$ cm rod has a tensile character. For the rest $10\leq x\leq L=30$, see the section of the rod also has a compressive character. In general $\varepsilon_x(x)$, it also has a nonlinear form.

Fig. 10 shows the distribution laws of three stress components:

1) $\sigma(x)$ is the thermoelastic stress component, defined by formula (30);

2) $\sigma_T(x)$ is the temperature stress component, defined by formula (33);

3) $\sigma_x(x)$ is the elastic stress component, determined by formula (35).

From Fig. 9, 10, it can be seen that they are proportional to the corresponding strain components. In this case, the proportionality coefficient is the modulus of elasticity of the rod material $E=2\cdot 10^6$ kG/cm^2.

Finally, Fig. 11 shows the distribution field of displacement of sections of the investigated rod of variable cross-section. It can be seen from the figure that all sections move from left to right in the direction of the Ox axis. This is due to the fact that the cross-sectional area of the left end of the rod where the heat flux of constant intensity q is applied is 4 times larger than the right one. The largest displacement amplitude corresponds to the cross-section of the rod with the coordinate $x=11.25$ cm. This is due to the occurrence of a large temperature $T(x=0)=112.059$ °C at the left end of the investigated rod of variable cross-section.

The Fig. 11 shows that all cross-sections move from left to right. This is also due to the large heat flux at the left end of the rod. The largest displacement is on the cross-section of the rod with the coordinate $x=11.25$ cm, as the displacement on both ends of the rod is equal to 0.

All the solutions obtained satisfy the fundamental laws of energy conservation; therefore, they are highly accurate. It is assumed that the developed methods, the computational algorithm and the software package ASIR 2.0 in Python will be useful in the design of power plants, internal combustion engines, jet engines.

The developed method can be used to study the applicability of the hypothesis of flat sections and before the appearance of plastic deformations, those within elastic deformations. Within these limitations, the results obtained will ensure convergence and accuracy.

In terms of the accuracy and convergence of the results obtained, this method is highly effective. But when sampling the studied rod for a large number of discrete elements, a large amount of memory and computation time are required. Although computational experiments show that the necessary accuracy is achieved with sufficiently small numbers of discrete elements.

7. Conclusions

1. A method for constructing spline approximating functions within the length of each discrete element of a rod of variable cross-section for determining the temperature field was developed, computational results and a graph were obtained.

The peculiarity of the proposed method consists in the fact that this method allows taking into account the existing natural boundary conditions at the level of the energy conservation law, taking into account the nonlinear variability of the cross-section. This solution approach makes it possible to take into account the piecemeal heterogeneity of the rod material. The developed method allows taking into account the simultaneous presence of several local heterogeneous heat sources and types of thermal insulation, making it possible to calculate thermal loads on a variable cross-section rod.

2. As a result of calculations, graphs of fields of all strain and stress components are obtained. The work does not take into account the dependence of the modulus of elasticity and the coefficient of thermal expansion on temperature. To do this, it is necessary to conduct appropriate experiments. Further study will address these shortcomings.

3. Using resolving systems of algebraic equations taking into account natural boundary conditions, displacement fields are calculated, a graph is plotted.

Conflict of interest

The authors declare that they have no conflict of interest regarding this study, whether financial, personal, authorship or any other that could affect the research and its results presented in this paper.

Financing

The study was carried out on the basis of State grant funding for scientific and technical projects of the Republic of Kazakhstan.

Data availability

Data will be provided upon reasonable request.

Acknowledgments

This work has been supported by the Kazakhstan Ministry of Education and Science via Research Grant Scheme No. AP05131093.

References

1. Timoshenko, S., Goodier. J. N. (1951). Theory of Elasticity. New York. Available at: http://parastesh.usc.ac.ir/files/1538886893033.pdf
2. Shorr, B. F. (2015). Thermoelasticity. Thermal Integrity in Mechanics and Engineering, 33–56. https://doi.org/10.1007/978-3-662-46968-2_2

3. Banerjee, B. (2006). Basic Thermoelasticity. doi: http://dx.doi.org/10.13140/RG.2.1.1144.2005
4. Saoud, S. (2009). Etude et Analyse Mathematique des Problems Non Lineaires Modelisant les Etats Thermiques d'un Superconducteur: Generalisation au Cas Tridimensionnel.
5. Griffith, G., Tucker, S., Milsom, J., Stone, G. (2000). Problems with modern air-cooled generator stator winding insulation. IEEE Electrical Insulation Magazine, 16 (6), 6–10. doi: https://doi.org/10.1109/57.887599
6. Li, Y. (2019). Investigation of Heat Transfer Characteristics on Rod Fastening Rotor. IOP Conference Series: Materials Science and Engineering, 677 (3), 032032. doi: https://doi.org/10.1088/1757-899x/677/3/032032
7. Shibib, K., Minshid, M., Alattar, N. (2011). Thermal and stress analysis in Nd: YAG laser rod with different double end pumping methods. Thermal Science, 15, 399–407. doi: https://doi.org/10.2298/tsci101201004s
8. Andreev, V., Turusov, R. (2016). Nonlinear modeling of the kinetics of thermal stresses in polymer rods. Advanced Materials and Structural Engineering, 719–722. doi: https://doi.org/10.1201/b20958-150
9. Belytschko, T., Liu, W. K., Moran, B. (2000). Nonlinear Finite Elements for Continua and Structures. John Wiley and Sons.
10. Wright, T. W. (2002). The Physics and Mathematics of Adiabatic Shear Bands. Cambridge University Press.
11. Batra, R. C. (2006). Elements of Continuum Mechanics. AIAA. doi: https://doi.org/10.2514/4.861765
12. Sukarno, D. H. (2021). Analysis of nuclear fuel rod temperature distribution using CFD calculation and analytical solution. PROCEEDINGS OF THE 6TH INTERNATIONAL SYMPOSIUM ON CURRENT PROGRESS IN MATHEMATICS AND SCIENCES 2020 (ISCPMS 2020). doi: https://doi.org/10.1063/5.0058888
13. El-Azab, J. M., Kandel, H. M., Khedr, M. A., El-Ghandoor, H. M. (2014). Numerical Study of Transient Temperature Distribution in Passively Q-Switched Yb:YAG Solid-State Laser. Optics and Photonics Journal, 04 (03), 46–53. doi: https://doi.org/10.4236/opj.2014.43007
14. Khany, S. E., Krishnan, K. N., Wahed, M. A. (2012). Study of Transient Temperature Distribution in a Friction Welding Process and its effects on its Joints. International Journal Of Computational Engineering Research, 2 (5), 1645.
15. Mishchenko, A. (2020). Spatially Structure Spatial Problem of the Stressed-Deformed State of a Structural Inhomogeneous Rod. IOP Conference Series: Materials Science and Engineering, 953, 012004. doi: https://doi.org/10.1088/1757-899x/953/1/012004
16. Hwang, J.-K. (2020). Thermal Behavior of a Rod during Hot Shape Rolling and Its Comparison with a Plate during Flat Rolling. Processes, 8 (3), 327. doi: https://doi.org/10.3390/pr8030327
17. Logan, D. L. (2012). A First Course in the Finite Element Method. CENGAGE Learning, 727–764.
18. Liu, Q., He, X. (2023). Thermal Analysis of Terfenol-D Rods with Different Structures. Micromachines, 14 (1), 216. doi: https://doi.org/10.3390/mi14010216
19. Gaspar Jr., J. C. A., Moreira, M. L., Desampaio, P. A. B. (2011). Temperature Distribution on Fuel Rods: A study on the Effect of Eccentricity in the Position of UO2 Pellets. 20-th International Conference «Nuclear Energy for New Europe». Available at: https://arhiv.djs.si/proc/nene2011/pdf/814.pdf